Variability of tropical upper tropospheric humidity 1979-1998

John Bates, Darren Jackson, Francois-Marie Breon, Zachary Bergen

JOURNAL OF GEOPHYSICAL RESEARCH, VOL. 106, NO. D23, PAGES 32,271–32,281, DECEMBER 16, 2001

Variability of tropical upper tropospheric humidity 1979–1998

John J. Bates
Environmental Technology Laboratory, NOAA, Boulder, Colorado, USA

Darren L. Jackson, Francois-Marie Bréon,[1] and Zachary D. Bergen
Cooperative Institute for Research in Environmental Sciences, University of Colorado, Boulder, Colorado, USA

Abstract. We update the time series of upper tropospheric humidity observations, begun in 1979 through May 1998, which includes the major El Niño event of 1997–1998. The intercalibration of different satellites is updated and compared to a physically based intercalibration. The results show excellent agreement and indicate that the main source of intersatellite bias is the known filter response function of the different instruments. Interannual variability of spatial fields is dominated by the major El Niño events in the 1979–1998 time period. Tropical average anomaly time series of upper tropospheric humidity, however, are dominated by a pronounced seasonal preference in extremes. Large deviations from the anomaly time series are twice as likely to occur in boreal winter and spring as in boreal summer and fall. During boreal winter and spring, the tropical basic state circulation permits the opening of a westerly wave duct such that midlatitude Rossby waves can propagate into the subtropics and tropics. We hypothesize that variation in the Rossby wave activity modulates the vertical water vapor flux and is responsible for large variations in the tropical upper tropospheric humidity time series.

1. Introduction

Studies of upper tropospheric water vapor variability have concentrated on understanding the water and energy balance in the subtropical dry zones (~10°N–30°N and 10°S–30°S). In the subtropics a relatively small change in upper tropospheric water vapor can lead to a relatively large change in the clear-sky outgoing longwave radiation (OLR) [*Spencer and Braswell*, 1997]. Discussions of the processes controlling the upper tropospheric water vapor distribution in the subtropics has focused on the interaction of the tropics with the subtropics and of the midlatitudes with the subtropics. This focus is because most theories have attempted to explain the steady state balance in the subtropics, and in the zonally averaged time-mean, the subtropics are regions of mean descending air. As a result, it is generally thought that the water vapor balance in the subtropics is not determined by local processes but is largely controlled by interactions with the tropics, such as detrainment from persistent regions of deep convection from the monsoons and intertropical convergence zones [*Salathe and Hartmann*, 2000], and interactions with midlatitudes, such as large-scale advection [*Pierrehumbert and Roca*, 1998].

There is increasing evidence, however, that these idealized theories for explaining the observed and modeled behavior of upper tropospheric water vapor in the tropics may be an oversimplification. An early study of the water and energy budget of the tropics [*Holland and Rasmusson*, 1973] found that the vertical eddy transport produced a large water vapor flux through the boundary layer and was positive up to the 500 hPa layer. More recently, work by *Sherwood* [1996] and *Pierrehumbert* [1998] have identified lateral mixing by transient eddies to be an important process in the water budget of the subtropical upper troposphere. Recent analysis of a general circulation model (Rind, personal communication) also indicates that vertical and horizontal mixing of water vapor by transient eddies is an important mechanism in moistening the subtropical upper troposphere.

In this investigation we examine the observed interannual variability for the past 20 years using satellite-derived upper tropospheric humidity observations. Satellite remote sensing observations do not provide direct information on the water vapor content (i.e., the water vapor mixing ratio). Rather, the satellite radiance observations, from filtered radiometers operating near the center of the water vapor absorption band at 6.7 μm, observe the water vapor and temperature over a relatively thick layer in the upper troposphere. As detailed by *Soden and Bretherton* [1996] and by *Stephens et al.* [1996], the satellite observations are most closely related to the relative humidity of a layer and the radiance-to-humidity relationship (for a more complete discussion, see *Jackson and Bates* [this issue]) results in a quantity called the upper tropospheric humidity (UTH).

In our analysis we consider whether some of the observed variability in UTH may be explained by the modulation of transient eddy activity in the tropics by changes in the seasonal to interannual basic state circulation. Basic state is a generic term for the time-mean circulation, in this case the monthly mean zonal wind speed at 200 hPa. We are primarily interested in examining the relationship between UTH and dynamical states in the subtropical regions. We do not examine the role of clouds and precipitation in the water and energy balance.

Since accurate long-term satellite data sets require the accurate intercalibration of a number of satellites, we first reexamine our intersatellite calibration methodology (detailed in the work of *Bates et al.* [1996], hereinafter referred to as BWJ) and compare it to an intersatellite calibration method based on

[1]On leave from the Laboratoire des Sciences du Climat et de l'Environnement, CEA/DSM/LSCE, Saclay, France.

Paper number 2001JD000347.
0148-0227/01/2001JD000347$09.00

known differences in filter response functions between satellites. Next, we analyze the observed interannual variability using several different satellite-derived data sets and a reanalysis data set. We then analyze the relationship between tropical-wide variability and regional variability. We find an important connection between the tropical-wide variability and the interaction between the tropical basic state circulation and the midlatitude circulation. We then present our conclusions.

2. Intercalibration of Water Vapor Radiances

A critical step in the use of observations from multiple satellites for climate analysis is the end-to-end calibration and intercalibration of all instruments used. Care must be taken to avoid spurious jumps in the time series due to changes in instrumentation or algorithms. For this work, we use data from the High Resolution Infrared Sounder (HIRS), which is a 20-channel filtered radiometer. The HIRS is one of a suite of sounding instruments that flies on the NOAA polar-orbiting satellites collectively referred to as the TIROS Operational Vertical Sounder (TOVS). It is difficult to quantify the effects of all sources of systematic errors that arise in merging data from similar instruments on differing satellites [*National Research Council (NRC)*, 2000]. The intercalibration process can be thought of as a three-step process [*Brest et al.*, 1997]: (1) the nominal calibration of each individual instrument, (2) the normalized calibration that adjusts all instruments to a baseline instrument, and (3) the absolute calibration that adjusts the normalized calibration to an independent reference standard. The nominal calibration of the HIRS instruments and all sources of random and systematic error associated with the use of the HIRS upper tropospheric water vapor channel are discussed in detail by BWJ. Random errors dominate this error budget.

For studies of interannual variability, such as this work, the systematic errors from instrument to instrument are significant (ranging from 0.05 to 0.95 K) and must be corrected. The intercalibration procedure, using the method known as empirical dynamic function (EDF), is described in BWJ and summarized here. Normally, there are two NOAA polar-orbiting satellites in orbit at any time and we use the overlap periods of the different satellites in the normalizing procedure. Each satellite passes over the same geographical area twice per day, morning-evening and afternoon-night. To apply the EDF procedure, interannual anomalies are first constructed for each satellite pass (morning, afternoon, evening, and night) and cumulative histograms of the anomaly data for each satellite, channel, and pass are constructed for time periods where data exist from both morning and afternoon satellites. Then the cumulative histograms for each period from the morning, afternoon, and night passes are adjusted to the evening pass using the EDF method. Adjustments are made to the evening pass since this pass has the smallest variance between cumulative histograms of the eight different satellite periods. Following the EDF anomaly adjustment, a mean bias adjustment is made with the EDF-adjusted anomalies for each period to eliminate small jumps between satellite periods. Mean bias adjustments are less than 0.3 K for HIRS channel 12 for all periods. Satellite periods with only one satellite have the two available passes adjusted to the evening pass using EDF information from the nearest period containing data from that satellite.

The absolute calibration of the HIRS upper tropospheric water vapor channel is complicated by a lack of high-quality in situ data. A complete and detailed description of all instruments and methods to measure upper tropospheric water vapor is available in a recent international assessment [*Kley et al.*, 2000]. Systematic biases between HIRS and other sources of upper tropospheric water vapor were found to be generally small (less than 1.5%), and the report concludes that there were no major inconsistencies in the HIRS UTH data that would preclude their use in climate and process studies.

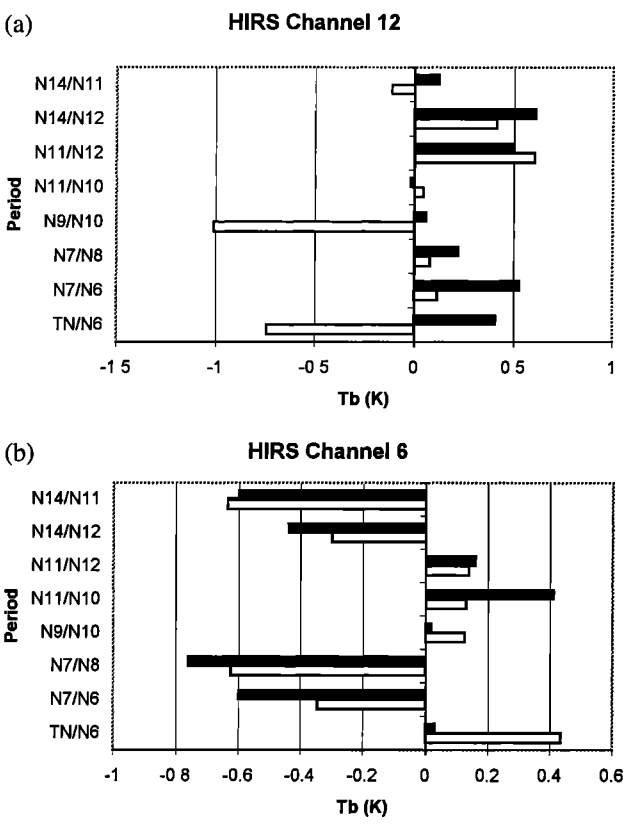

Figure 1. Satellite-to-satellite systematic biases for HIRS (a) channels 12 and (b) 6 computed from forward physical principles (solid bar) and from empirical dynamic function analysis (open bar).

We are continuing, however, to examine and quantify the two major sources of systematic error in the HIRS data set. These are the systematic differences from instrument to instrument which are probably attributable to small changes in the filter response functions and changes in the cloud detection procedure over time. To assess the systematic error due to the filter response functions, we have compared the BWJ empirical calibration with a forward modeled calculation. To perform the forward modeled calculation, we use the instrument spectral response functions, a sample set of atmospheric temperature and moisture profiles (from the TIGR atmospheres [*Chaboureau et al.*, 1998]) and a radiative transfer model (MODTRAN 3.7 [*Berk et al.*, 1989]). The convolution of the response function with the transmittance for a variety of atmospheres provides an a priori estimate of the systematic biases from instrument to instrument.

The results of these calculations are presented in Figure 1. In this figure we compare the systematic bias between each set of overlapping satellites using our empirical method (the open bars) and a method based solely on the physical differences in

the filter functions for the different instruments (the solid bars). We do not expect an exact match between the empirical and the forward modeled intersatellite biases because the sample atmospheres will not be an exact match with the observed atmospheres. In most cases, however, the agreement between the empirical and the forward-modeled intersatellite biases is on the order of only a few tenths of a degree. This is an excellent agreement and lends credibility to our assertion that most of the intersatellite bias is attributable to known differences in the filter response functions from instrument to instrument. There are, however, a few notable exceptions. Disagreements of ~1 K are found in HIRS channel 12 between the NOAA-9 and the NOAA-10 instruments and between the TIROS-N and NOAA-6 instruments. The difference between TIROS N and NOAA 6 is attributed to a relatively short overlap between the two instruments. The difference between NOAA 9 and NOAA 10 is not clear, but we believe it is attributable to errors in the specification of the filter response function for the NOAA-9 instrument. We are reexamining the filter response specification of NOAA 9 to ensure that the manufacturer correctly specified it.

These results are in conflict with those BWJ reported in an earlier attempt to perform a physically based assessment of intersatellite biases [*Bates et al.*, 1996]. For that work BWJ had used a different radiative transfer model, RTTOV-3 [*Eyre*, 1991]. A recent comparison of this model with others in the water vapor absorption band [*Soden et al.*, 2000] revealed that the RTTOV-3 model had large systematic and random errors relative to the other models. In this same intercomparison, MODTRAN was found to have very low systematic and random errors. Thus we believe that our poor results in our earlier attempt to physically model the intersatellite biases in HIRS channel 12 were due to the use of an inaccurate radiative transfer model and not to the uncertainties in the filter functions.

As detailed by *Jackson and Bates* [this issue], the empirical relationship between HIRS channel 12 and UTH can be improved by using temperature data from HIRS channel 6. For this reason we also performed similar calculations for this channel. We find (Figure 1b) even better agreement between the empirical intersatellite calibrations for this channel. Thus we conclude that our empirical intersatellite bias adjustment is highly consistent with known physical differences in the different instruments, lending credibility to the adjustment procedure.

This and all prior UTH work using the NOAA satellites have used the clear column radiance (CCR) data set produced operationally by National Environmental Satellite Data and Information Service (NESDIS). Thus far it has not been possible to assess systematic biases that may have arisen due to small changes in the operational cloud detection procedure over time. After April 1998 the CCR data set produced by NESDIS changed substantially, and so we do not use the CCR data after that time. We are in the process of computing a clear column radiance data set from the raw (level 1b) TOVS data with a consistent cloud detection scheme, updated quality control, and longer data records. This project, called the TOVS Radiance Pathfinder Project, involves a massive reprocessing of over 1.5 terabytes of data but will be available soon and will allow us to minimize this source of systematic error.

It should be noted that it is common practice in discussing data from filtered radiometers such as the HIRS instrument to use the terms radiance and brightness temperature interchangeably even though they have different units. This is because the central frequency for each channel on a filtered radiometer is defined exactly, so that through the use of the Planck function, we can unambiguously equate radiance and brightness temperature.

3. Observed Interannual Variability

One way to examine the processes that relate the surface temperature, deep convection, upper tropospheric water vapor, and clear-sky outgoing longwave radiation is to examine the largest interannual signals. Within the tropics the largest signals are related to El Niño-Southern Oscillation (ENSO) events. We have therefore plotted several tropical interannual anomaly time series and their spatial patterns for the past 20 years. The time series will be discussed first. The time series of sea surface temperature (SST) anomalies in the central equatorial Pacific, the Niño-3 area (Figure 2c), and the Southern Oscillation index (SOI) (the Darwin-Tahiti pressure difference) are highly correlated with the leading principal component time series of precipitation and HIRS UTH (Figure 2d). Variability in the precipitation and the UTH are synchronous. A measure of the intensity of the tropical Hadley cell overturning (Figure 2e) has been computed from NCEP reanalysis data [*Kalnay*, 1996]. This meridional mass stream function [*Peixoto and Oort*, 1992] has been computed for the northern winter season (December–January–February) when the effects of ENSO warm events are most pronounced in the Northern Hemisphere midlatitudes and only the maximum value of the zonal-mean cross section for the Hadley cell has been plotted. This index shows that the Hadley cell intensifies during ENSO warm events and that it was very intense during the 1982–1983, 1994–1995, and 1997–1998 warm events. Thus in terms of all these indices, the ENSO warm events of 1982–1983 and 1997–1998 stand out in terms of the largest signals.

Figure 2a shows the leading empirical orthogonal function (EOF) of anomalous precipitation [*Xie and Arkin*, 1997] during the past 20 years. During ENSO warm events, precipitation is enhanced in the central and eastern equatorial Pacific and precipitation is decreased in the western equatorial Pacific and in the South Pacific convergence zone. Figure 2b shows the leading EOF of interannual variability of HIRS UTH. The spatial pattern shows an increase in the upper tropospheric humidity over the central and eastern equatorial Pacific, over western Australia and extending west into the southern Indian Ocean, and over smaller regions in the North and South Atlantic. Decreases in the upper tropospheric humidity are found in the north and south subtropics of the Pacific, over the western equatorial Pacific over northeast Brazil, and over the Gulf of Guinea. Of these, however, the largest decrease is found over the subtropical North Pacific between Hawaii and Baja California. This is an area where the upper tropospheric humidity is already low, so this is where we would expect changes in UTH to have a large impact on clear-sky OLR.

ENSO events have often been described as simply a rearrangement of the existing hydrological and circulation features within the tropical atmosphere. The variations of the mass stream function shown above indicate this is not the case and that ENSO warm events result in a fundamentally different basic state of the tropical circulation. It is therefore of interest to examine the tropical averaged responses of UTH and clear-sky OLR for interannual signals. Tropical average (30°N–30°S) time series of sea surface temperature (SST) [*Reynolds*, 1994],

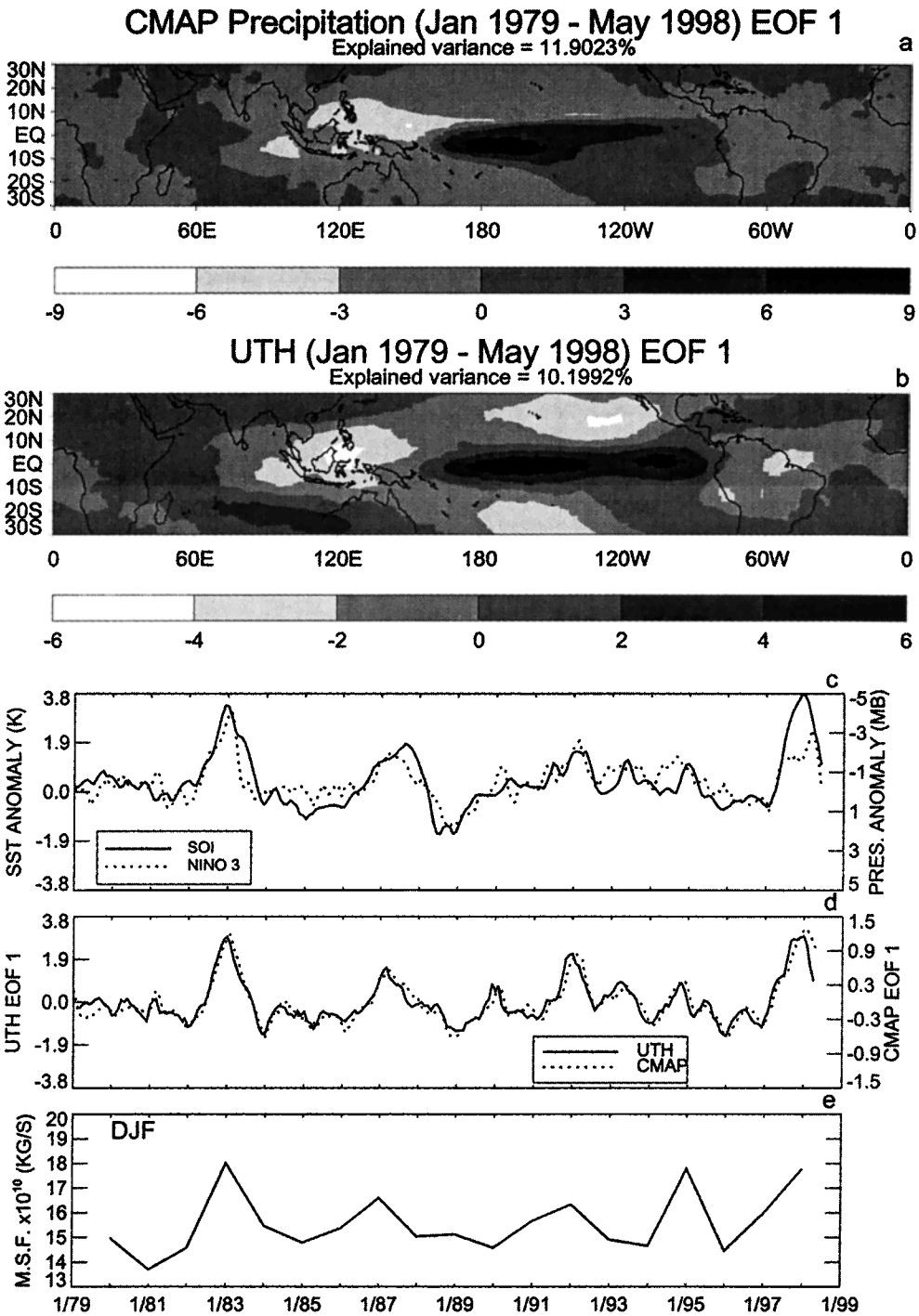

Figure 2. Leading empirical orthogonal function for (a) CMAP precipitation interannual anomalies, (b) UTH interannual anomalies, (c) ENSO indices for SST interannual anomalies in Niño-3 region and Southern Oscillation Index, (d) principal component of leading EOF for CMAP and UTH, and (e) meridional stream function for DJF season.

tropospheric temperature from the TOVS Microwave Sounding Unit (MSU channel 2) [*Christy et al.*, 1998, 1995], UTH, and clear-sky OLR from CLERA [*Slingo et al.*, 1998] and CERES [*Wielicki et al.*, 1998] are shown in Figure 3. Since these indices are now tropical averages, the values of the variability are rather small because they are the result of much larger anomalies of opposite sign. (Because of the short record of the CERES data, we have computed CERES anomalies with respect to the long-term mean of the CLERA data. Since we are interested in relative variations, we have also removed a bias between the CLERA and the CERES data for the base month of January 1998 when the tropical anomalies of both data sets were near zero.) Also included in these plots are SST indices for the tropical Pacific regions sensitive to ENSO, the Niño-4 region in the western equatorial Pacific, and the Niño-3 region in the central equatorial Pacific. Table 1 shows the cross

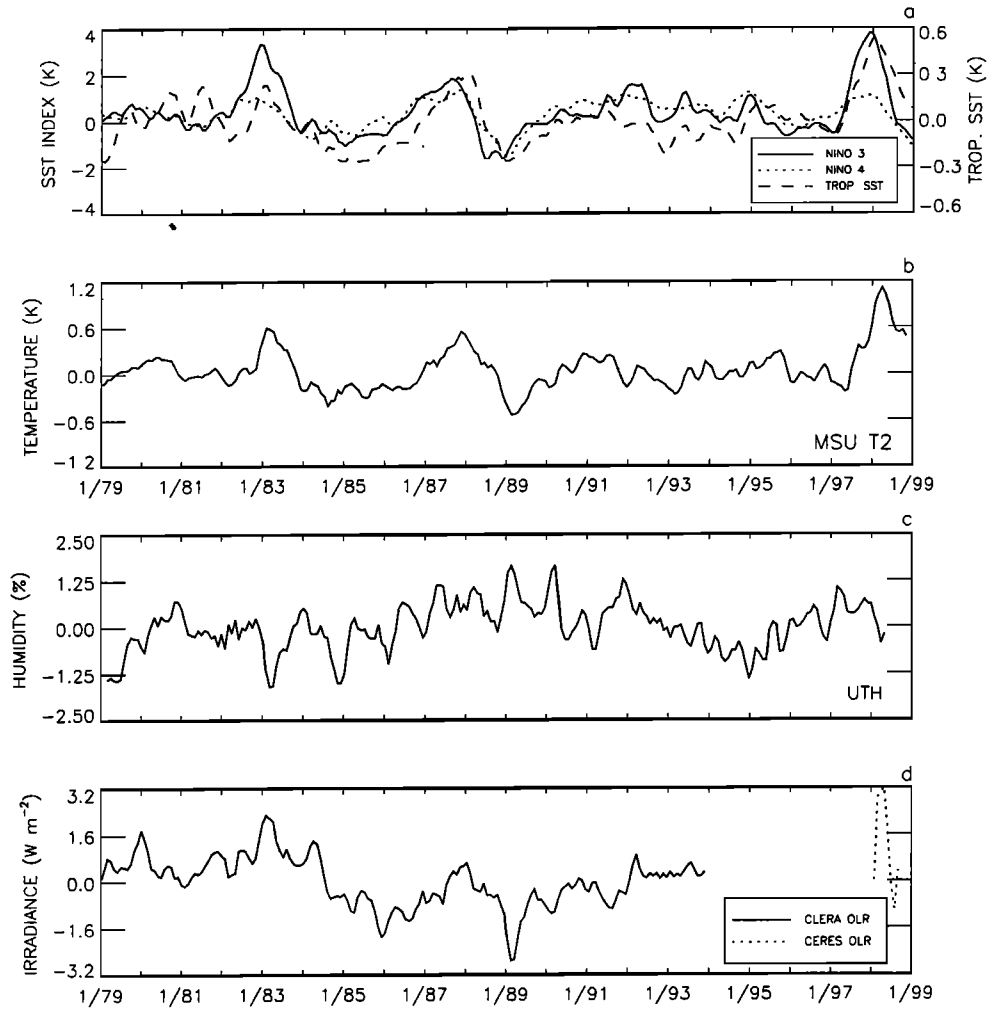

Figure 3. Interannual anomaly time series of indices for tropical region (30°N–30°S) for (a) SST (and SST for Niño regions 3 and 4; note change of scale), (b) MSU tropospheric temperature, (c) UTH, and (d) clear-sky OLR from CLERA and CERES.

correlations for these variables and the significance of the cross correlations accounting for the lag-one persistence in each time series. The tropospheric temperatures are correlated to SSTs in the Niño-3 region at 0.60 (significance level between 80 and 85%). *Yulayeva and Wallace* [1994] find that lower tropospheric temperatures are more highly correlated with Niño-3 SST at a 1-month lag. Correlations are lower between Niño-3 SST and UTH (−0.30) and clear-sky OLR (0.50), and significance levels are below 80%. There is a significant negative correlation between the UTH and the clear-sky OLR time series (−0.60 significance greater than 99%). This is to be expected because HIRS channel 12 is a main predictor of clear-sky OLR [*Ellingson et al.*, 1994], and HIRS channel 12 was used in the ECMWF reanalysis [*McNally and Vesperini*, 1996]. Slight differences in these time series are found and are attributed to the use of HIRS radiances only over the oceans in the ECMWF reanalysis (G. Kelly, personal communication).

Table 1. Cross-Correlation Table for Tropical, Zonally Averaged Niño-3 SST, MSU-2 Tropospheric Temperature, UTH, and Clear-Sky OLR[a]

	MSU 2	UTH	CLERA Clear-Sky OLR
Niño-3 SST	0.60 (>80%)	−0.30 (<80%)	0.50 (<80%)
MSU-2		−0.40 (>90%)	0.56 (>90%)
UTH			0.60 (>99%)

[a]Significance levels, accounting for lag-one autocorrelation between time series are given in parentheses.

Although the correlations between SST and UTH and between SST and clear-sky OLR are not significant, there does appear to be some association between the different time series. The two most extreme negative values of UTH (most extreme positive value of clear-sky OLR) occur during the mature phase of the extreme ENSO events of 1982–1983 and 1997–1998. The most extreme positive value of UTH (most extreme negative value of clear-sky OLR) occurs during the extreme cold event of 1989. These UTH extremes are of much shorter duration than the SST and tropospheric temperature anomalies. This suggests that anomalies in tropical UTH and clear-sky OLR occur on both seasonal and interannual timescales in contrast to SST and tropospheric temperature, which show only interannual variability.

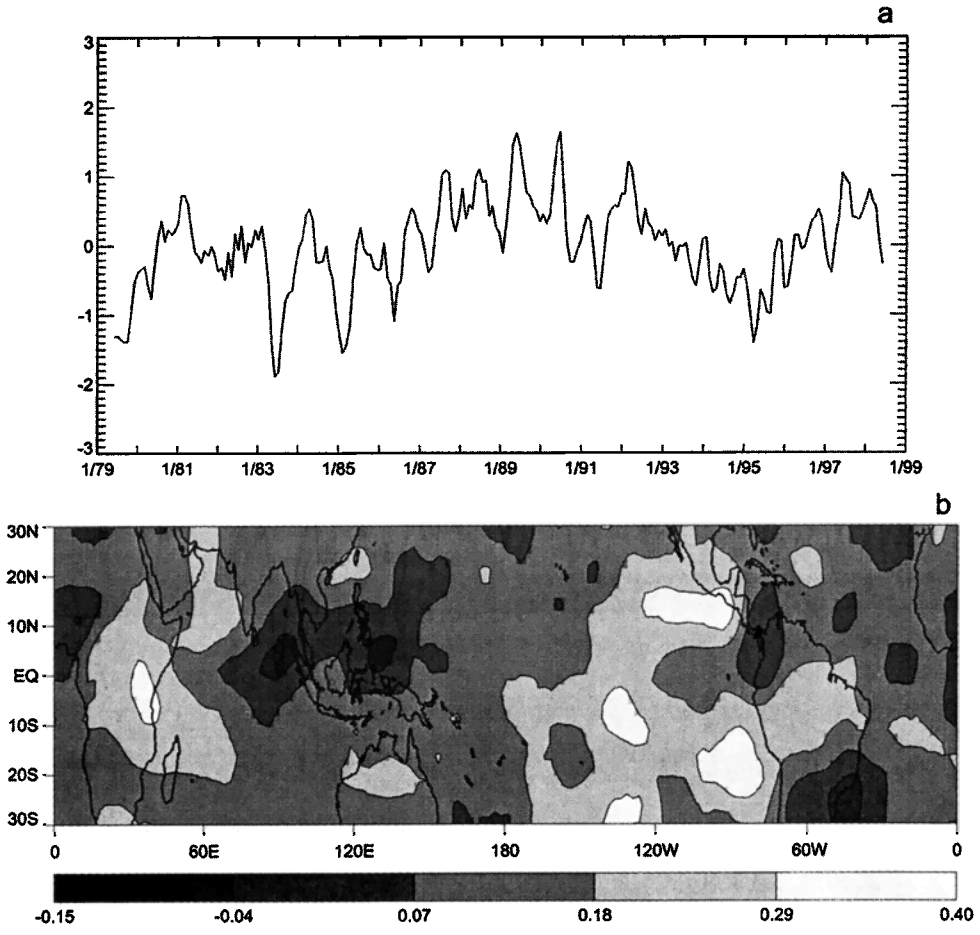

Figure 4. Interannual anomaly time series of (a) tropical UTH (30°N–30°S) and (b) one-point correlation map.

In an attempt to quantify which regions of the tropics contribute most significantly to the tropical wide time series of Figure 3c, we computed a one-point correlation map between the tropical-wide UTH time series and the UTH time series at each grid point. This map (Figure 4) shows that the largest contribution comes from the eastern Pacific. Several studies have indicated that transient eddy activity is high in this area [*Kiladis and Weickmann*, 1997] and that the transient eddies are associated with large plumes of moisture [*Iskenderian*, 1995]. This transient eddy activity has a strong seasonal component [*Kiladis and Weickmann*, 1997] and also shows a strong interaction with ENSO events [*Matthews and Kiladis*, 1999]. Thus variations in eddy activity are a possible candidate to explain some extremes of the tropical interannual anomaly time series of UTH and clear-sky OLR.

To further examine the relationship between the UTH time series and the seasonal to interannual variability, we identified all months with UTH variability exceeding 0.7%. A histogram of those months within the seasonal cycle revealed that extremes of UTH are twice as likely to occur in the boreal winter and spring (38 in December–January–February (DJF) and March–April–May (MAM)) as in boreal summer and fall (19 in June–July–August (JJA) and September–October–November (SON)). This seasonal preference for tropic-wide extremes in the UTH time series again suggests we should examine the possible contribution of transient eddy activity in producing the extremes.

4. Dynamical Analysis of Transient Eddy Activity

To examine the changes in transient eddy activity in this region during the large warm event of 1982–1983 and the large cold event of 1989–1990, we employed the dynamical analysis of 200 hPa winds as outlined by *Kiladis* [1998]. The horizontal E vector is a pseudovector constructed by calculating time-mean covariances between the perturbation zonal (u') and meridional (v') wind components:

$$\vec{E} = \left(\overline{v'^2 - u'^2},\ \overline{-u'v'}\right). \quad (1)$$

The term $\overline{v'^2 - u'^2}$ is a measure of the mean anisotropy of Rossby waves. For example, if v'^2 is consistently larger than u'^2, the Rossby waves are preferentially elongated in the meridional direction and the E-vector points eastward. The term $\overline{-u'v'}$ is the negative of the time-mean northward flux of westerly momentum associated with perturbations. Together, the two components approximate the preferred direction of the group velocity of the Rossby waves using suitable approximations, including the assumption of quasi-geostrophy. For

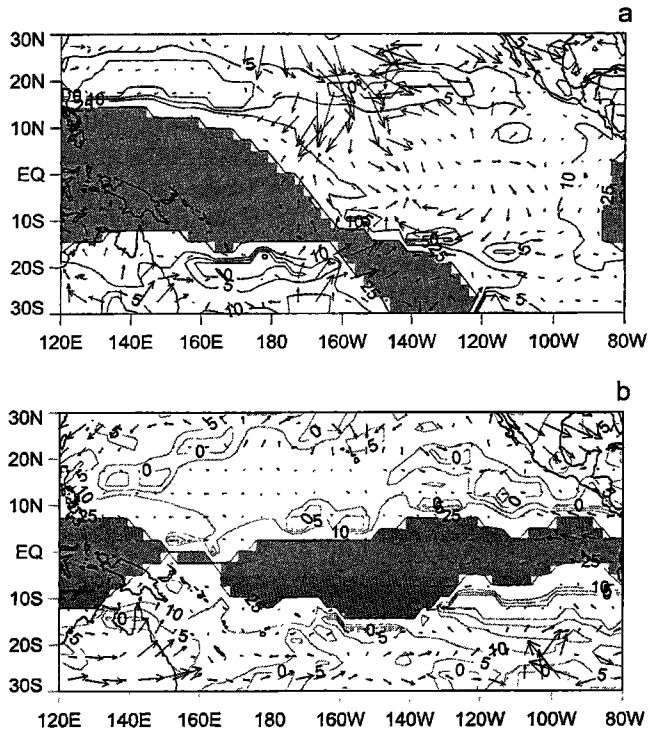

Figure 5. Mean fields for (a) February 1989 and (b) April 1983. The 200-hPa total stationary Rossby wave number is contoured at zonal wave numbers 0, 5, 10, 15, 20, and 25, and contours greater than 25 are shaded. Also shown are the high-frequency (6–25 days) 200-hPa E-vectors. The largest vector shown is 125 m^{-2} s^{-2}.

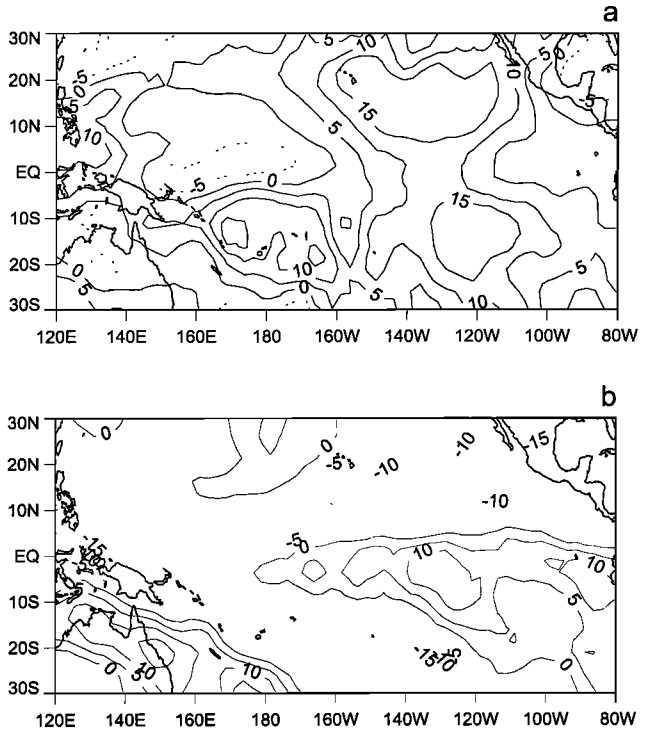

Figure 6. Monthly mean UTH anomaly fields for (a) February 1989 and (b) April 1983.

this work we use the NCEP reanalysis data and bandpass filter for 6- to 30-day transients.

Another useful diagnostic for representing the mean background state in which the transients are embedded is the stationary Rossby wave number:

$$K_s = \left(\frac{\beta_*}{\bar{U}}\right)^{1/2}, \tag{2}$$

where

$$\beta_* = \beta - \frac{\partial^2 \bar{U}}{\partial y^2} \tag{3}$$

is the meridional gradient of absolute vorticity associated with the basic flow, $\bar{U}$ is the monthly mean 200 hPa zonal wind, and $\beta = \partial f/\partial y$ is the meridional gradient of planetary vorticity. K_s is the total wave number at which a barotropic Rossby wave is stationary at a particular location in a given background zonal flow. Low values of the stationary Rossby wave number (below about 10) indicate regions of strong eddy activity, and high values (above 15) indicate regions of weak eddy activity.

E-vectors and the stationary Rossby wave number were computed for all months and plots of the minima UTH (April 1983), and maxima UTH (February 1989) months are shown in Figure 5. In the Northern Hemisphere, midlatitude interactions with the tropics are greatest in boreal winter and spring when transient Rossby wave activity with periods between 5 and 30 days is at a peak. During strong cold events, such as 1989 (Figure 5a), tropical convection occurs only over the far western Pacific Ocean since the western Pacific warm pool shrinks and moves to the west during cold events. In the tropical upper troposphere near the equator, this creates strong westerly winds in the outflow from this convection over the central and eastern Pacific. This allows the opening of a westerly duct in the eastern Pacific and supports propagation of Rossby waves deep into the subtropics [*Webster and Holton*, 1982]. This is evidenced in Figure 5a where values of stationary Rossby wave numbers less than 10 are found in the regions between the dateline and the west coast of South America. Large values of E-vectors pointing toward the equator near Hawaii are indicative of equatorially propagating Rossby waves from the midlatitudes into the subtropics. As shown by *Kiladis* [1998], the Rossby waves then propagate to the east and are associated with large plumes of moisture extending from near Hawaii to the U.S. West Coast sometimes dubbed the "pineapple express."

Conversely, during the large warm event of 1982 (Figure 5b), deep convection extends far to the east in the equatorial Pacific Ocean. Upper tropospheric westerlies over the equator weaken dramatically or even reverse in the central and eastern Pacific. This is confirmed by calculations of the stationary Rossby wave number for these events. Large values of the stationary Rossby wave number are found over the eastern tropical Pacific, effectively shutting down the westerly duct. Virtually, no E-vectors pointing toward the equator are found in this month, indicating an almost complete absence of Rossby waves in the subtropical North Pacific. Figure 6 shows the UTH monthly mean anomaly fields for these two months. During February 1989 (Figure 6a) we find large regions of positive UTH anomalies exceeding 15% over the subtropical eastern Pacific, and conversely, during April 1983 (Figure 6b) we find large negative anomalies. Thus there is strong evidence that the large variability of transient eddy activity in the sub-

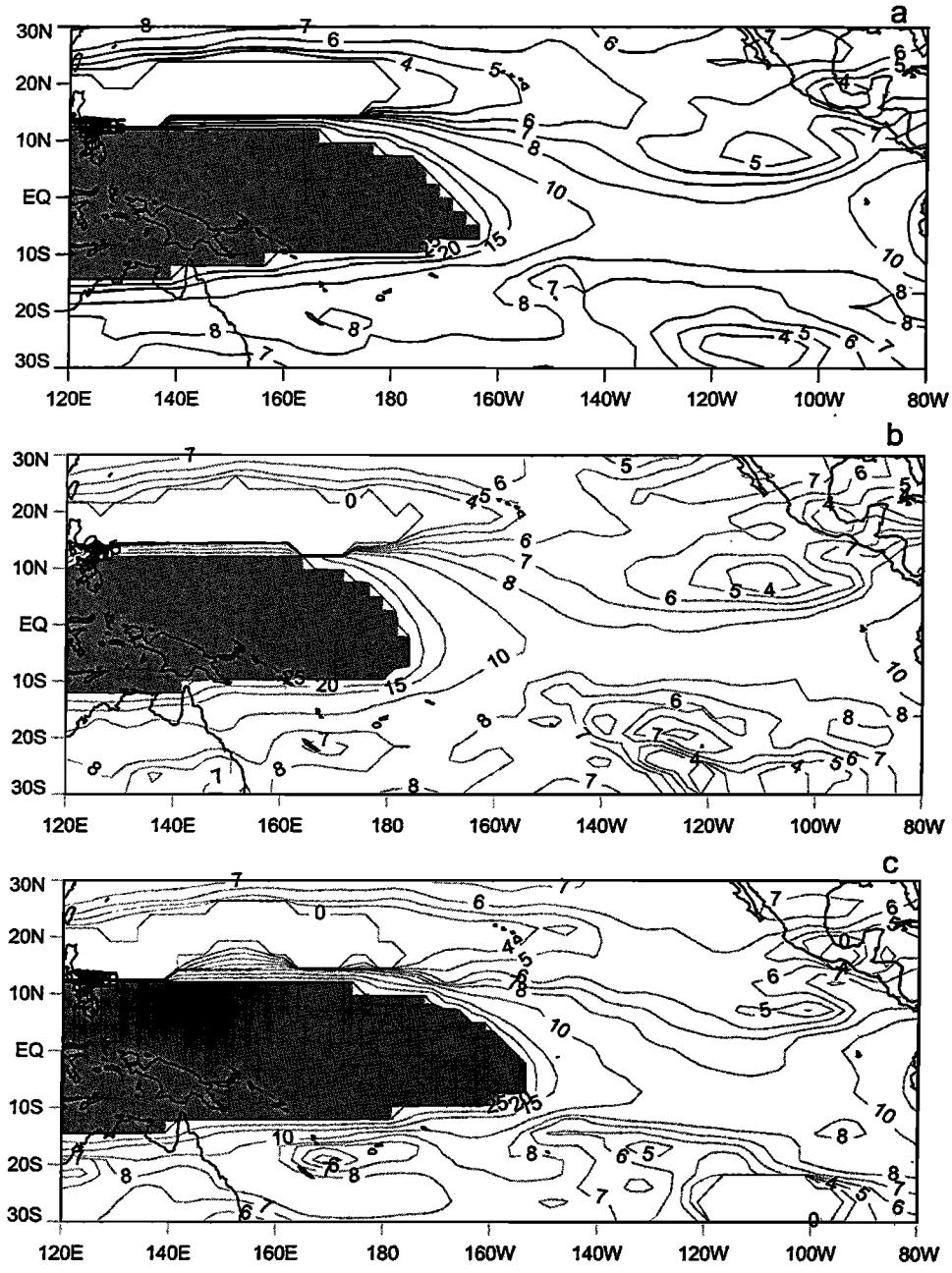

Figure 7. The 200-hPa total stationary Rossby wave number for boreal winter (a) mean, (b) UTH anomaly months greater than 0.7%, and (c) UTH anomaly months less than −0.7%.

tropical North Pacific plays an important role in explaining the tropic-wide extremes of UTH and clear-sky OLR interannual anomalies.

We examined the statistical characteristics of the relationship between the UTH extremes and the Rossby wave activity by computing the seasonal mean Rossby stationary wave number. We computed the mean of all months within the season for only those months within the season with tropical average UTH anomalies greater than 0.7% and UTH anomalies less than −0.7%. For the boreal winter season (Figure 7) we find that low values of the stationary Rossby wave number extend farther west versus the mean along the equator when UTH anomalies exceed 0.7% (Figure 7b) and are found farther east when UTH anomalies are less than −0.7% (Figure 7c). The situation is even more dramatic for the boreal spring season (Figure 8). Thus the westerly duct is larger when UTH anomalies exceed 0.7% and is much smaller when UTH anomalies are less than −0.7%.

We have illustrated these two different basic state upper tropospheric circulation regimes schematically in Figure 9. When the westerly duct is open (Figure 9a), outflow from deep convection in the equatorial west Pacific is strong, producing strong westerly winds across the central and eastern equatorial Pacific. This in turn creates a minimum of speed shear in the mean zonal wind and allows Rossby waves to propagate from midlatitudes deep into the subtropics (strong eddy activity). Although we must still quantify the relative roles of vertical versus horizontal transient water vapor flux, it is easiest to

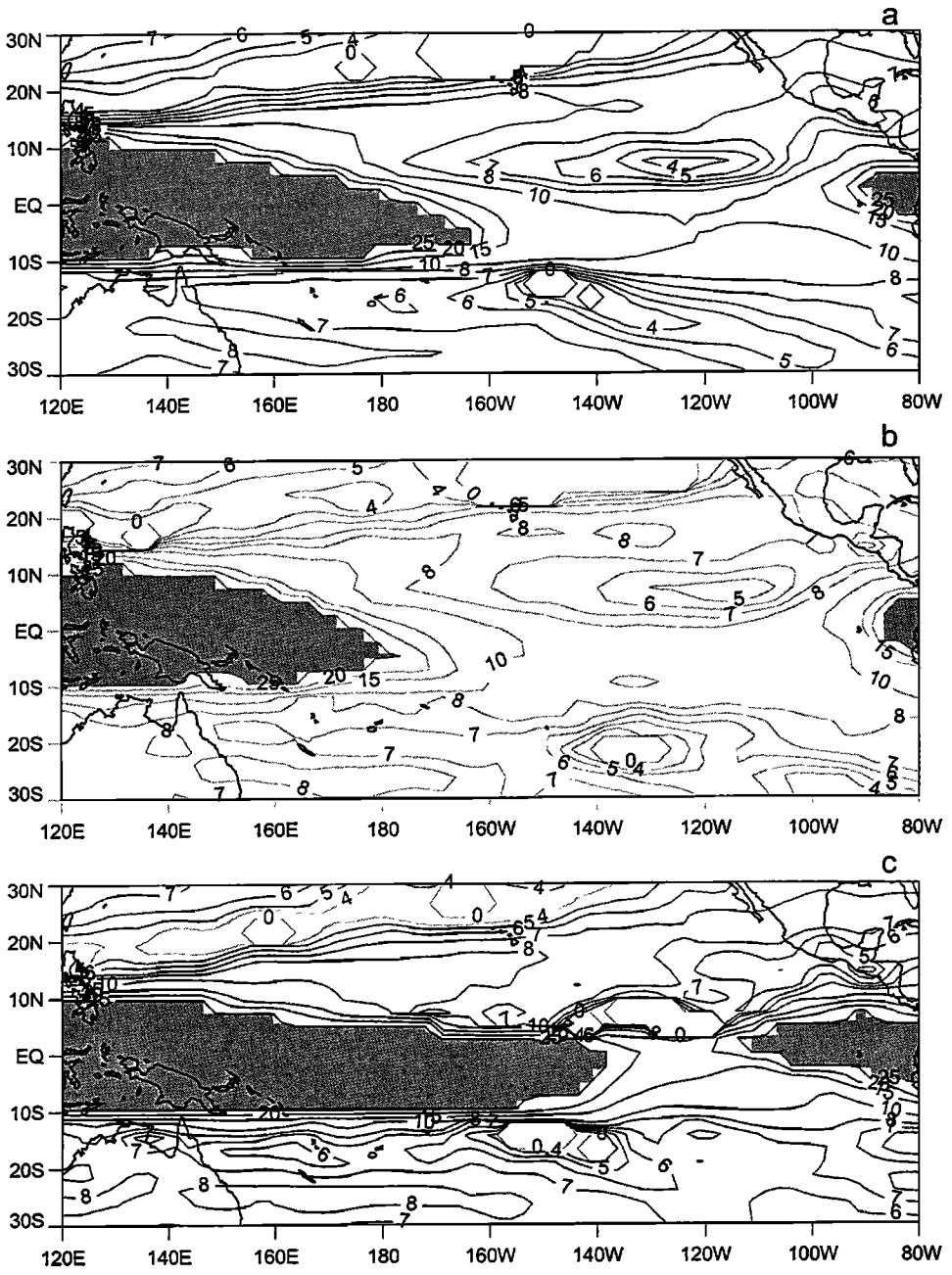

Figure 8. The 200-hPa total stationary Rossby wave number for boreal spring (a) mean, (b) UTH anomaly months greater than 0.7%, and (c) UTH anomaly months less than −0.7%.

change the water vapor by vertical flux since the water vapor mixing ratio gradient is much larger in the vertical than the horizontal. The westerly duct is the smallest when deep convection extends far into the central and eastern equatorial Pacific (Figure 9b). In this case there is only weak westerly outflow in the far eastern Pacific and weak winds or even easterlies in the central Pacific. This leads to strong shear of the zonal winds in the subtropics and inhibits the propagation of Rossby waves (no eddies).

Although we find a relationship between the extremes of tropic-wide UTH and the variability of the westerly duct in the tropical Pacific Ocean, our initial examination was driven by trying to explain the extremes in the UTH time series for the very large ENSO warm event of 1982–1983 and the cold event of 1989. The UTH time series, however, is noisy, and there are several more modest ENSO events in the time series. Is there a general relationship between ENSO events and the UTH time series? We find that UTH maximums occur most frequently when SST anomalies in the Niño-3 region are near normal and UTH minimums occur when SST anomalies are near normal or positive. Thus there does not appear to be a more general relationship between a simple ENSO index and the UTH extremes.

5. Conclusions

The clear column radiance data set for HIRS channel 12 and for UTH have been updated and now extend from January

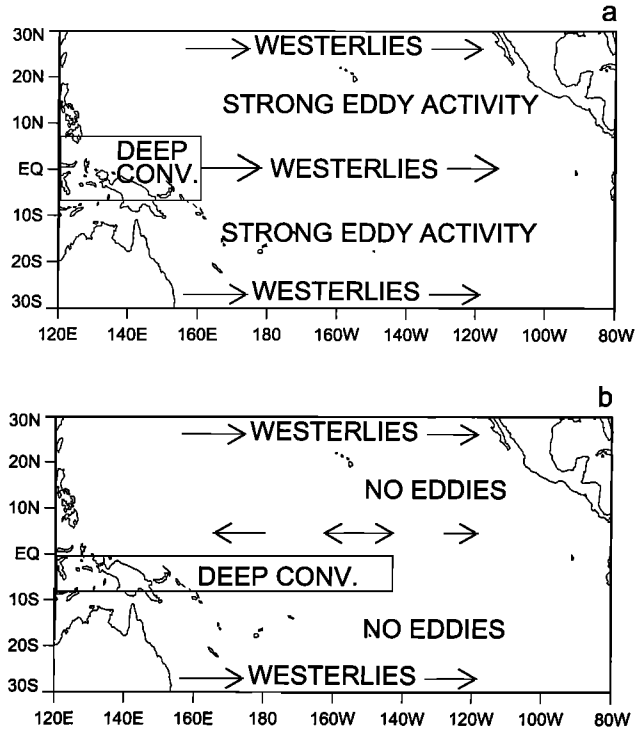

Figure 9. Schematic of the basic state circulation features for (a) the open westerly duct and (b) the closed westerly duct.

1979 to May 1998. Future updates will be produced from the HIRS level 1b data set for all HIRS channels as part of the TOVS Radiance Pathfinder Project. The intersatellite calibration, using the technique of empirical dynamic function analysis, has been performed for the additional overlap periods of the NOAA-14/12 and NOAA-11/14 satellites. We have validated this empirical intersatellite calibration by computing the intersatellite biases using first-principle physics based on a sample of atmospheric profiles and the measured filter response functions. This comparison suggests that for most of the instruments the empirically derived biases are consistent with those expected from physical changes in the instrument filter response functions from instrument to instrument, the only exception being the overlap period for the NOAA-9 and NOAA-10 instruments.

Strong tropical and midlatitude interactions occur preferentially during northern winter and spring due to the presence of upper tropospheric westerly winds in both the central and the eastern equatorial Pacific and in the midlatitudes. Midlatitude eddies, or Rossby waves, can propagate into the subtropics and tropics under such circumstances. The vertical and horizontal motions associated with these waves advect moisture both vertically and horizontally, moistening the normally dry subtropics. This moistening is greatly enhanced during the ENSO cold event of 1989–1990. During this time, convection was confined to the far western equatorial Pacific producing a long fetch of upper tropospheric westerlies in the central and eastern equatorial Pacific and thus enhancing the transient eddy activity in the tropics. During the extreme ENSO warm event of 1982–1983, convection occurred over the central and eastern equatorial Pacific greatly diminishing, or even reversing, the westerly winds in the upper troposphere. This closed the westerly duct and greatly inhibited the propagation of transient eddies into the subtropics.

We find these results also apply more generally to the relationship between the tropical basic state circulation during boreal winter and spring. When there are positive tropic-wide UTH anomalies exceeding 0.7%, the westerly duct is larger than normal, and when UTH anomalies are less than −0.7%, the westerly duct is smaller than normal.

Much work remains to be done to further explore this hypothesis. We are currently conducting a study of the water budget to quantify the influence of the different components of the moisture flux on the net water budget of the subtropics. We are interested in both the stationary and the transient eddy fluxes and the vertical and horizontal components. The influence of clouds cannot be ignored, and we would like to conduct a more complete analysis of the net radiation budget with and without clouds. Within the deep tropics, the organization of convection over the Pacific is determined not by a simple SST index but rather by the SST gradient field. Since the organization of convection is related to the tropical basic flow, and hence the amount of eddy activity in the subtropics, accurate prediction of the SST gradient field is a key parameter for both improved modeling of seasonal to interannual variations and climate change.

Acknowledgment. George Kiladis suggested we look at the connection between Rossby wave action in the east Pacific and variability in upper tropospheric humidity.

References

Bates, J. J., X. Wu, and D. L. Jackson, Interannual variability of upper-tropospheric water vapor band brightness temperature, *J. Clim.*, *9*(2), 427–438, 1996.

Berk, A., L. S. Bernstein, and D. C. Robertson, *MODTRAN: A Moderate Resolution Model for LOWTRAN 7*, Spectral Sciences, Inc., Burlington, Mass., 1989.

Brest, C. L., W. B. Rossow, and M. D. Roiter, Update of radiance calibrations for ISCCP, *J. Atmos. Oceanic Technol.*, *14*(5), 1019–1109, 1997.

Chaboureau, J. P., A. Chedin, and N. A. Scott, Relationship between sea surface temperature, vertical dynamics, and the vertical distribution of atmospheric water vapor inferred from TOVS observations, *J. Geophys. Res.*, *103*, 23–34, 1998.

Christy, J. R., R. W. Spencer, and R. T. McNider, Reducing noise in the MSU daily lower-tropospheric global temperature data set, *J. Clim.*, *8*(4), 888–902, 1995.

Christy, J. R., R. W. Spencer, and E. S. Lobl, Analysis of the merging procedure for the MSU daily temperature time series, *J. Clim.*, *11*, 2016–2041, 1998.

Ellingson, R. G., L. Hai-Tien, D. Yanuk, and A. Gruber, Validation of a technique for estimating outgoing longwave radiation from HIRS radiance observations, *J. Atmos. Oceanic Technol.*, *11*(2), 357–365, 1994.

Eyre, J. R., *A Fast Radiative Transfer Model for Satellite Sounding Systems*, pp. 26, Eur. Cent. for Medium-Range Weather Forecasts, Reading, England, 1991.

Holland, J. Z., and E. M. Rasmusson, Measurements of the atmospheric mass, energy, and momentum budgets over a 500 km square of tropical ocean, *Mon. Weather Rev.*, *101*, 44–53, 1973.

Iskenderian, H., A 10-year climatology of Northern Hemisphere tropical cloud plumes and their composite flow patterns, *J. Clim.*, *8*, 1630–1637, 1995.

Jackson, D. L., and J. J. Bates, Upper tropospheric humidity algorithm assessment, *J. Geophys. Res.*, this issue.

Kalnay, E., The NCEP/NCAR 40-year reanalysis project, *Bull. Am. Meteorol. Soc.*, *77*(3), 437–448, 1996.

Kiladis, G. N., Observations of Rossby waves linked to convection over the eastern tropical Pacific, *J. Atmos. Sci.*, *55*(3), 321–335, 1998.

Kiladis, G. N., and K. M. Weickmann, Horizontal structure and sea-

sonality of large-scale circulations associated with submonthly tropical convection, *Mon. Weather Rev.*, *125*(9), 1997–2008, 1997.

Kley, D., J. M. Russell III, and C. Phillips, *SPARC Assessment of Upper Tropospheric and Lower Stratospheric Water Vapour*, pp. 305, Geneva, Stratospheric Process. and Their Role in Clim., Switzerland, 2000.

Matthews, A. J., and G. N. Kiladis, Interactions between ENSO, transient circulation, and tropical convection over the Pacific, *J. Clim.*, *12*(10), 3062–3074, 1999.

McNally, A. P., and M. Vesperini, Variational analysis of humidity from the TOVS radiances, *Q. J. R. Meteorol. Soc.*, *122*, 1521–1544, 1996.

National Research Council (NRC), *Reconciling Observations of Global Temperature Change*, pp. 85, Natl. Acad. of Sci., Washington, D. C., 2000.

Peixoto, J. P., and A. H. Oort, *Physics of Climate*, 434 pp., Am. Inst. of Phys., New York, 1992.

Pierrehumbert, R. T., Lateral mixing as a source of subtropical water vapor, *Geophys. Res. Lett.*, *25*, 151–154, 1998.

Pierrehumbert, R. T., and R. Roca, Evidence for control of Atlantic subtropical humidity by large-scale advection, *Geophys. Res. Lett.*, *25*(24), 4537–4540, 1998.

Reynolds, R. W. S., T. M. Smith, Improved sea surface temperature analysis using optimum interpolation, *J. Clim.*, *7*, 929–937, 1994.

Salathe, E. P., and D. L. Hartmann, Subsidence and upper-tropospheric drying along trajectories in a general circulation model, *J. Clim.*, *13*, 257–263, 2000.

Sherwood, S. C., Maintenance of the free-tropospheric tropical water distribution, part II, Simulation by large-scale advection, *J. Clim.*, *9*, 2919–2934, 1996.

Slingo, A., J. A. Pamment, and M. J. Webb, A 15-year simulation of the clear-sky greenhouse effect using the ECMWF reanalyses: fluxes and comparisons with ERBE, *J. Clim.*, *11*(4), 690–706, 1998.

Soden, B. J., and F. P. Bretherton, Interpretation of TOVS water vapor radiances in terms of layer-average relative humidities: Method and climatology for the upper, middle, and lower troposphere, *J. Geophys. Res.*, *101*, 9333–9343, 1996.

Soden, B., et al., An intercomparison of radiation codes for retrieving upper tropospheric humidity in the 6.3 micron band: A report from the 1st GVAP Workshop, *Bull. Am. Meteorol. Soc.*, *81*, 797–808, 2000.

Stephens, G. L., D. L. Jackson, and I. Wittmeyer, Global observations of upper-tropospheric water vapor derived from TOVS radiance data, *J. Clim.*, *9*(2), 305–326, 1996.

Webster, P. J., and J. R. Holton, Cross-equatorial response to middle-latitude forcing in a zonally varying basic state, *J. Atmos. Sci.*, *39*(4), 722–733, 1982.

Wielicki, B. A., et al., Clouds and the Earth's Radiant Energy System (CERES): Algorithm overview, *IEEE Trans. Geosci. Remote Sens.*, *36*(4), 1127–1136, 1998.

Xie, P., and P. Arkin, Global precipitation: A 17-year monthly analysis based on gauge observations, satellite analysis, and numerical model outputs, *Bull. Am. Meteorol. Soc.*, *78*(11), 2539–2558, 1997.

Yulayeva, E., and J. M. Wallace, The signature of ENSO in global temperature and precipitation fields derived from the Microwave Sounding Unit, *J. Clim.*, *7*(11), 1719–1730, 1994.

J. J. Bates, Environmental Technology Laboratory, NOAA, 325 Broadway, Boulder, CO 80305, USA. (john.j.bates@noaa.gov)

Z. D. Bergen, F.-M. Bréon, and D. L. Jackson, Cooperative Institute for Research in Environmental Sciences, NOAA, Mail Code R/ET7, University of Colorado, Boulder, CO 80305-3328, USA. (darren.l.jackson@noaa.gov)

(Received January 9, 2001; revised August 9, 2001;
accepted August 15, 2001.)